Nanoscale Horizons

Check for updates

Photodoping of graphene with long-lived electrons by interfacing with Janus WSSe

Ting Zheng, [ab] Yu-Chuan Lin,*[cd] Zhenhua Ni, [ae] Kai Xiao[c] and Hui Zhao *[b]

The performance of semiconductor optoelectronic devices depends on efficient photodoping of active materials, where optical excitation generates photocarriers. Despite more than two decades of research, efficient photodoping in graphene remains elusive due to the formation of neutral excitons with ultrashort lifetimes. Here, by interfacing graphene with a Janus WSSe monolayer, we achieve unipolar photodoping of graphene with long-lived carriers. The Janus monolayer was synthesized via selenium implantation of WS_2 monolayers grown by chemical vapor deposition. We fabricated the heterostructure by transferring a mechanically exfoliated graphene monolayer onto the Se-terminated side of WSSe. Through photoluminescence and transient absorption spectroscopy, we demonstrate that photoexcited electrons in WSSe transfer efficiently to graphene, while a portion of the photoexcited holes remains confined in WSSe due to its built-in electric field. This charge separation leads to a net electron population in graphene. These electrons exhibit extended lifetimes due to spatial separation from their recombination partners, offering a promising route to enhancing the performance of graphene-based optoelectronic devices.

New concepts

This work presents a novel photodoping strategy for monolayer graphene that overcomes fundamental limitations imposed by its ultrashort carrier lifetime (picosecond scale). In contrast to conventional transition metal dichalcogenide (TMD)/graphene heterostructures where rapid transfer and recombination of both photocarriers occurs in graphene, the Janus/graphene heterostructure in this work exhibits a unique asymmetric charge transfer mechanism. The intrinsic out-of-plane electric field of a Janus WSSe layer can cause efficient electron transfer to graphene while confining holes in WSSe. This engineered charge separation results in a long-lived net electron population in graphene, thereby addressing the challenge of optical doping. This simple bilayer architecture achieves the directional and persistent charge separation, paving the way for innovative graphene-based optoelectronic devices and high-performance photodetectors.

optoelectronic devices and leverage graphene's exceptional charge transport properties, it is crucial to generate long-lived charge carriers through optical excitation.

Combining graphene with other two-dimensional (2D) semiconductors in van der Waals heterostructures offers a promis-

Introduction

Graphene is widely regarded as a promising optoelectronic material due to its high charge carrier mobility[1,2] and broadband optical absorption.[3] However, photoexcitation of graphene leads to the formation of tightly bound, charge-neutral excitons[4] with short recombination lifetimes on the order of picoseconds. To enhance the performance of graphene-based

[a] School of Physics, Southeast University, Nanjing 211189, China

[b] Department of Physics and Astronomy, The University of Kansas, Lawrence, Kansas 66045, USA. E-mail: huizhao@ku.edu

[c] Center for Nanophase Materials Sciences, Oak Ridge National Laboratory, Oak Ridge, Tennessee 37831, USA

[d] Department of Materials Science and Engineering, National Yang Ming Chiao Tung University, Hsinchu, Taiwan. E-mail: ycl194@nycu.edu.tw

[e] School of Electronic Science & Engineering, Southeast University, Nanjing 211189, China

Hui Zhao

Congratulations to Nanoscale Horizons on its 10th anniversary! We are honored to have contributed four publications to this leading journal over the past decade. We deeply appreciate its commitment to scientific excellence, rapid publication, and high-impact research centered on new concepts. It has been a pleasure to engage with this vibrant journal—as readers, authors, and reviewers—dedicated to innovation at the frontiers of nanoscience. The new horizons revealed through its pages have shaped the research directions of many groups, including our own. We wish Nanoscale Horizons continued growth and success in the years to come.
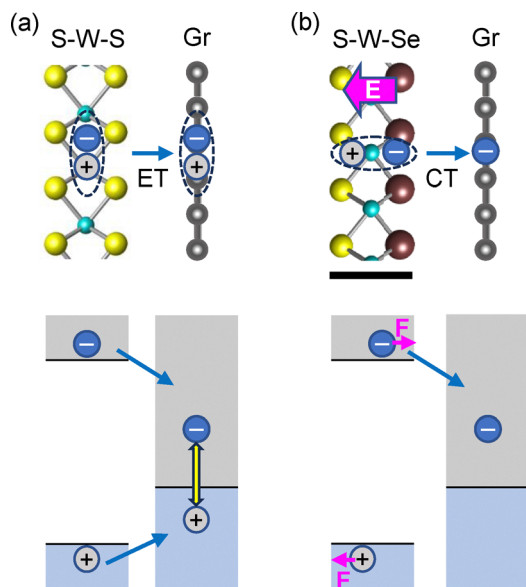
Fig. 1 Schematic illustrations of the atomic structures (top panels) and band alignments (bottom panels) of WS₂/graphene (a) and Janus WSSe/graphene (b) heterostructures. In WS₂/graphene, energy transfer (ET) to graphene is followed by rapid recombination. In Janus WSSe/graphene, the built-in electric field (E) exerts opposing forces (F) on electrons and holes, enabling electron transfer while suppressing hole transfer to graphene, thereby resulting in a net charge transfer.

ing approach to enhancing performance and addressing these challenges.[5] Recent efforts have focused on heterostructures composed of transition metal dichalcogenides (TMDs) and graphene, where the TMD serves as the light absorption layer and graphene as the charge transport layer.[6–11] However, because semiconducting TMDs and graphene form a type-I band alignment, both electrons and holes photoexcited in the TMD layer transfer to graphene, resulting in no net charge transfer (CT) but only energy transfer (ET), as shown in Fig. 1(a). Additionally, recent experiments have shown that the transferred electrons and holes rapidly recombine in graphene within a few picoseconds,[12–19] making it difficult to harness these photocarriers for high-efficiency devices. To achieve optical injection of charge carriers in graphene, multilayer heterostructures with carefully engineered band alignments are often required.[20,21]

Here, we demonstrate that a heterostructure composed of graphene and a Janus TMD enables optical injection of charge carriers into graphene. A Janus TMD monolayer, consisting of a transition metal atomic layer sandwiched between two different chalcogen layers, has been recently synthesized.[22–26] Its asymmetric lattice structure gives rise to a built-in out-of-plane electric field, as illustrated in Fig. 1(b). In previous works, we showed that this built-in field in Janus MoSSe and WSSe monolayers can displace photoexcited electrons and holes in opposite directions,[27] thereby influencing interlayer charge transfer dynamics.[28] In this study, as shown in Fig. 1(b), we hypothesize that in a Janus WSSe/graphene heterostructure, the built-in field exerts opposing forces on electrons and holes, promoting electron transfer while suppressing hole transfer into graphene and thus enabling a net electron injection into graphene.

Results and discussion

Fig. 2(a) presents an optical microscope image of the sample, showing individual Janus WSSe and graphene (Gr) regions, along with their heterostructure region, enabling direct comparisons. The monolayer thickness of the graphene flake was confirmed by Raman spectroscopy, as shown in Fig. 2(b), where the 2D peak is higher than the D peak.[29,30]

To probe photocarrier behavior, photoluminescence (PL) measurements were performed on different regions of the sample using continuous-wave laser excitation at 1.96 eV with an incident power of 10 μW. The laser spot was focused to approximately 0.5 μm using a microscope objective lens. When the excitation spot was positioned on the Janus WSSe region, a strong PL peak at 1.85 eV was observed [red curve in Fig. 2(c)], consistent with previous reports.[27] However, when the excitation spot was moved to the heterostructure region, the PL intensity was quenched by a factor of 28. This strong quenching indicates that photoexcited carriers in WSSe efficiently transfer to graphene before recombining in WSSe. This observation confirms both the high quality of the interface and the occurrence of efficient charge or energy transfer. We note that the features in the range of 1.90–1.95 eV are artifacts introduced by the filter used to block the 1.96 eV laser.

We first conducted transient absorption measurements to study the photocarrier dynamics in the heterostructure sample using a 3.02 eV pump and a 0.83 eV probe. In this configuration, the pump excites both layers, while the probe senses only carriers in graphene, as its photon energy is well below the optical bandgap of WSSe (1.85 eV). The pump fluence used in
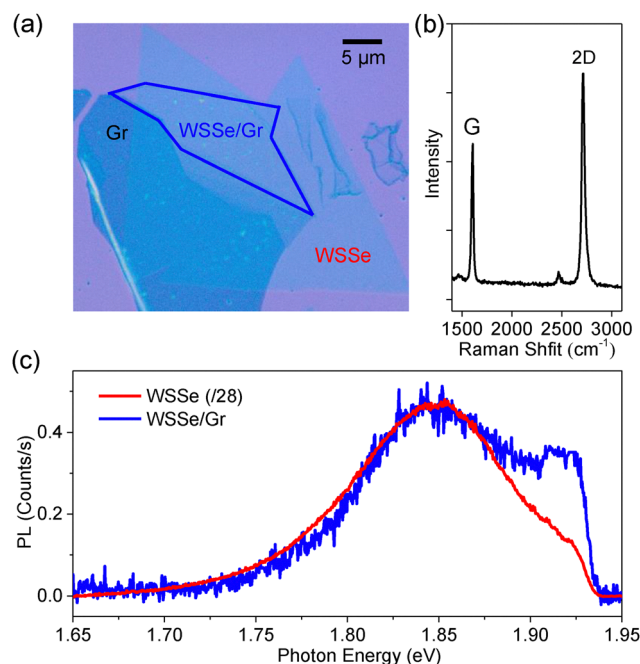
Fig. 2 (a) Optical microscope image of the sample. The Janus WSSe/graphene heterostructure region is outlined in blue. (b) Raman spectrum of the graphene monolayer. (c) Photoluminescence (PL) spectra of the Janus WSSe monolayer and the heterostructure regions.
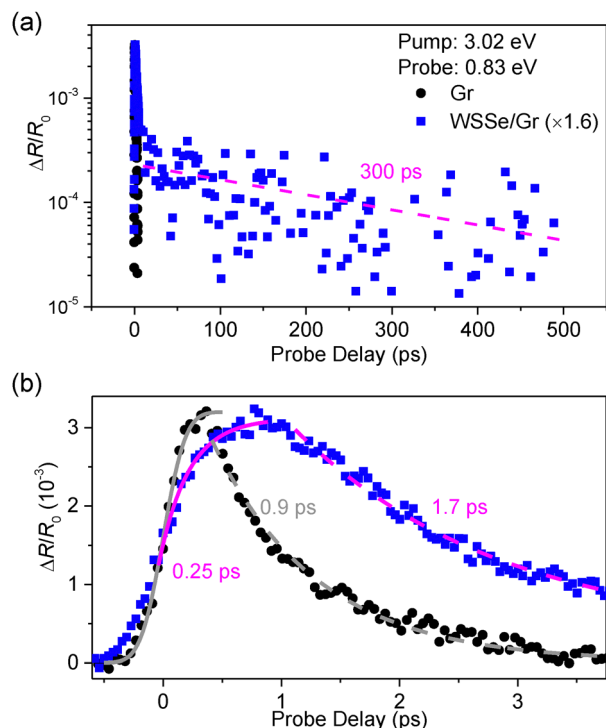
Fig. 3 (a) Differential reflectance of graphene (Gr) and the Janus WSSe/graphene heterostructure, measured using a 3.02 eV pump and 0.83 eV probe pulses. (b) Zoomed-in view of the early probe delay region.

this measurement was 7.4 μJ cm^{-2}, corresponding to an estimated peak carrier density of 4.6×10^{11} cm^{-2}, based on an absorbance of 0.067 at 3.02 eV.[27] The blue symbols in Fig. 3(a) show the measured differential reflectance signal, $\Delta R/R_0 = (R - R_0)/R_0$, where R and R_0 are the reflectance of the sample with and without the pump, respectively. The most notable feature is that a portion of the signal persists for several hundred picoseconds. Due to the low signal-to-noise ratio, we were unable to reliably extract a decay time constant through fitting. Nevertheless, the magenta dashed line in Fig. 3(a) represents an exponential decay function with a time constant of 300 ps, which captures the overall trend. Although the exact decay time is uncertain, the presence of a long-lived component is evident. Notably, such a feature is absent in previous measurements of conventional WS$_2$/graphene heterostructures.[14] When the same measurement was repeated on bare graphene, the signal decayed within a few picoseconds (black symbols). We note that the signal magnitudes from the two measurements are not directly comparable due to differences in pump absorption and carrier-induced transient absorption efficiency.

To analyze the photocarrier dynamics, Fig. 3(b) presents the same data as in (a), but focused on early probe delays. The signal from graphene rises to a peak on a time scale limited by the instrument response. The solid gray curve represents the integral of a Gaussian function with a standard deviation of 0.15 ps, corresponding to the intensity cross-correlation of the pump and probe pulses. The signal then decays exponentially with a time constant of 0.9 ± 0.1 ps, confirming the ultrashort

lifetime of photocarriers in graphene. In contrast, the rise of the signal from the heterostructure is slower. Since most carriers are photoexcited in the WSSe layer due to its higher absorbance, this rise reflects the transfer of carriers to graphene. Using a simple model, $N(t) = N_0[1 - \exp(-t/\tau_T)]$, where N and N_0 represent the time-dependent and peak densities of transferred carriers in graphene, respectively, we extracted a carrier transfer time of $\tau_T = 0.25 \pm 0.03$ ps. The majority of the signal then decays exponentially with a time constant of 1.7 ± 0.2 ps, along with the long-lived component discussed earlier in Fig. 3(a).

We interpret these features as arising from the influence of the built-in electric field in WSSe on the photocarrier transfer process. Upon photoexcitation in WSSe, both electrons and holes can immediately transfer to graphene. Simultaneously, the built-in field can drive some holes away from the interface, hindering their transfer to graphene. As a result of these competing processes, a fraction of the photoexcited holes remains in WSSe, while all electrons and most holes transfer to graphene. The transferred holes rapidly recombine with electrons in graphene, leaving behind a net population of electrons in graphene and holes in WSSe. The observed 1.7 ps lifetime is longer than the 0.9 ps lifetime measured in bare graphene. This difference may be attributed to variations in the dielectric environment, as the graphene layers rest on Janus WSSe and SiO$_2$, respectively. Slightly extended carrier lifetimes in graphene within TMD/graphene heterostructures have been reported previously.[14] Based on the ratio between the peak signal and the long-lived signal, we estimate that the net electron density injected in graphene is approximately 5% of the total carrier density.

To confirm the above interpretation, we next compared the Janus WSSe/graphene heterostructure with the bare WSSe monolayer region by directly probing the photocarrier population in WSSe. We first studied the carrier dynamics in the WSSe monolayer using a 2.03 eV pump pulse with a peak fluence of 3.7 μJ cm^{-2} to inject photocarriers. The peak carrier density was estimated to be approximately 3.2×10^{10} cm^{-2} using an absorbance of 0.007.[27] A 1.84 eV probe, near the optical bandgap of WSSe, was used to monitor the carrier population. The red triangles in Fig. 4(a) represent the measured differential reflectance signal, which can be well fit by a biexponential decay function, $\Delta R/R_0 = A_1 \exp(-t/\tau_1) + A_2 \exp(-t/\tau_2)$, with decay time constants of $\tau_1 = 5.5 \pm 0.8$ ps and $\tau_2 = 41 \pm 5$ ps (purple curve). The shorter time constant, τ_1, is attributed to exciton formation and hot exciton cooling, while the longer time constant, τ_2, can be reliably assigned to exciton recombination.

When the same measurement was performed on the heterostructure region, the signal exhibited a rapid decay. An exponential fit yields a decay time constant of 0.9 ± 0.2 ps (magenta curve), which is attributed to the transfer of the majority of photocarriers from WSSe to graphene. This result is consistent with the dynamics observed in Fig. 3 and supports our earlier interpretation. In addition to the fast decay, the signal also exhibits a long-lived component. As in Fig. 3(a), we include a 300 ps decay function (magenta dashed line) to illustrate the long-time behavior, which aligns well with the measured data.
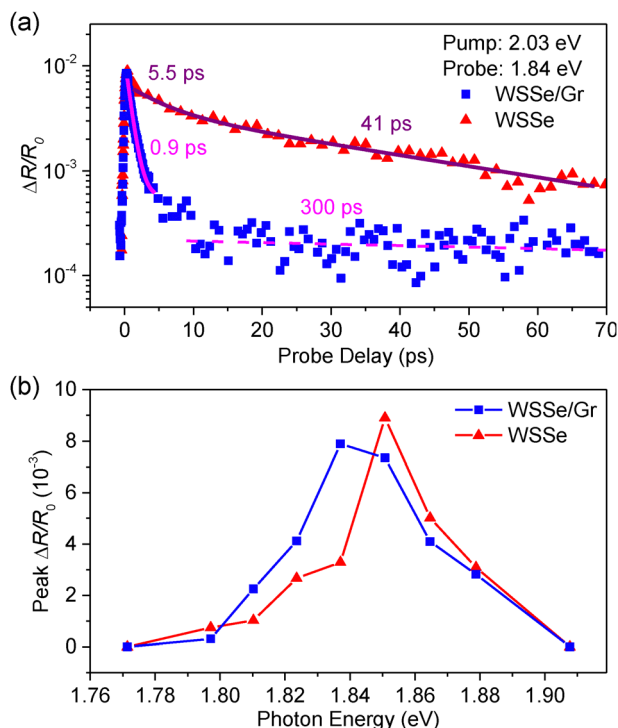
Fig. 4 (a) Differential reflectance of the Janus WSSe monolayer and the Janus WSSe/graphene heterostructure regions, measured using a 2.03 eV pump and 1.84 eV probe pulses. (b) Peak differential reflectance as a function of probe photon energy.

We attribute this long-lived component to holes that were excited in WSSe but did not transfer to graphene due to the built-in electric field. Notably, this component accounts for approximately 5% of the peak signal, in good agreement with the proportion of the long-lived signal observed when probing the graphene layer [Fig. 3]. We note that this percentage reflects the competition between the immediate transfer of holes to graphene upon photoexcitation and the effect of the built-in electric field. Within the range of our study, this ratio remains independent of the injected carrier density.

To further confirm that the probe monitors carriers in WSSe, we measured the differential reflectance of both samples while tuning the probe photon energy. As shown in Fig. 4(b), both samples exhibit a pronounced resonant feature near the optical bandgap of WSSe, which is approximately 1.85 eV, consistent with the PL spectrum in Fig. 2(c).

Conclusion

In summary, we have demonstrated, using transient absorption and photoluminescence spectroscopy, that a heterostructure composed of Janus WSSe and graphene enables optical electron doping of graphene. This effect arises from the built-in electric field in the Janus layer, which exerts opposite forces on electrons and holes, resulting in asymmetric charge transfer. Unlike heterostructures based on conventional TMDs, where both photoexcited electrons and holes transfer to graphene and

thus yielding no net charge transfer, a fraction of the photo-excited holes in WSSe remains confined. This leads to a net electron population in graphene with an extended lifetime.

This optical charge doping in a simple bilayer heterostructure offers a promising strategy for enhancing the performance of graphene-based ultrathin optoelectronic devices. For example, it enables dynamic photo-modulation of charge carrier density in graphene photodetectors or transistors without the need for electrostatic gating or chemical doping. Such non-invasive and reversible doping mechanisms are advantageous for ultrafast photonic switches and light-driven logic devices. Furthermore, the ability to engineer charge carrier dynamics *via* the built-in electric field of Janus layers in van der Waals heterostructures opens new avenues for designing multifunctional 2D material platforms tailored for next-generation optoelectronics and quantum technologies.

Experimental section

Sample fabrication

Janus WSSe monolayers were obtained *via* selenium implantation into WS_2 monolayers. The WS_2 monolayers were first synthesized by chemical vapor deposition on a SiO_2/Si substrate, which was mounted on a heater located 10 cm away from a selenium pellet target inside a cylindrical stainless-steel chamber. A 248 nm pulsed KrF excimer laser, operating at a repetition rate of 1–5 Hz with a pulse width of 25 ns, was used to ablate the Se target in an Ar atmosphere. The laser produced a rectangular beam spot measuring 1.25 mm × 4.5 mm and delivered an energy fluence of 1.0 J cm^{-2} at the target surface. The heater temperature was controlled by a PID system with a precision of ±2 °C and a ramp rate of approximately 30 °C per minute. High-quality Janus WSSe monolayers were obtained under optimized conditions of 20 mTorr pressure and a substrate temperature of 30 °C.[24,27,31]

To fabricate Janus WSSe/graphene heterostructures, graphene flakes were obtained by mechanically exfoliating bulk graphite crystals (2D semiconductors) using adhesive tape *via* the push-and-peel method, followed by transfer onto a poly-dimethylsiloxane substrate. A selected graphene monolayer was then transferred onto a Janus WSSe monolayer. The resulting heterostructure was annealed at 200 °C in an Ar atmosphere for 4 hours to promote interface quality and adhesion.

Transient absorption measurements

The transient absorption measurements were performed using a setup based on an 80 MHz Ti:sapphire laser and an optical parametric oscillator (OPO). The desired pump and probe wavelengths were obtained from the Ti:sapphire laser output, its second harmonic generated using a nonlinear optical crystal, and the signal output of the OPO. The pump and probe pulses were co-focused onto the sample using a microscope objective lens. The reflected probe beam was detected by a photodiode and processed by a lock-in amplifier referenced to a mechanical chopper that modulated the pump beam at approximately 3 kHz.

Author contributions

Y.-C. L. and H. Z. conceived the idea. H. Z. and Z. H. N. supervise the investigation. T. Z. performed the optical spectroscopy measurements. Y.-C. L. fabricated the samples under supervision of K. X. All authors contributed to experimental results interpretation, data analysis, and manuscript preparation.

Conflicts of interest

There are no conflicts to declare.

Data availability

The data that support the findings of this study are openly available in KU ScholarWorks at **https://kuscholarworks.ku.edu**.

Acknowledgements

Notes and references

1 K. S. Novoselov, A. K. Geim, S. V. Morozov, D. Jiang, Y. Zhang, S. V. Dubonos, I. V. Grigorieva and A. A. Firsov, *Science*, 2004, **306**, 666–669.

2 A. K. Geim and K. S. Novoselov, *Nat. Mater.*, 2007, **6**, 183–191.

3 R. R. Nair, P. Blake, A. N. Grigorenko, K. S. Novoselov, T. J. Booth, T. Stauber, N. M. R. Peres and A. K. Geim, *Science*, 2008, **320**, 1308.

4 L. Yang, J. Deslippe, C.-H. Park, M. L. Cohen and S. G. Louie, *Phys. Rev. Lett.*, 2009, **103**, 186802.

5 J. P. Shi, M. X. Liu, J. X. Wen, X. B. Ren, X. B. Zhou, Q. Q. Ji, D. L. Ma, Y. Zhang, C. H. Jin, H. J. Chen, S. Z. Deng, N. S. Xu, Z. F. Liu and Y. F. Zhang, *Adv. Mater.*, 2015, **27**, 7086.

6 W. J. Yu, Y. Liu, H. Zhou, A. Yin, Z. Li, Y. Huang and X. Duan, *Nat. Nanotechnol.*, 2013, **8**, 952–958.

7 L. Britnell, R. M. Ribeiro, A. Eckmann, R. Jalil, B. D. Belle, A. Mishchenko, Y.-J. Kim, R. V. Gorbachev, T. Georgiou, S. V. Morozov, A. N. Grigorenko, A. K. Geim, C. Casiraghi, A. H. C. Neto and K. S. Novoselov, *Science*, 2013, **340**, 1311–1314.

8 W. J. Yu, Z. Li, H. L. Zhou, Y. Chen, Y. Wang, Y. Huang and X. F. Duan, *Nat. Mater.*, 2013, **12**, 246–252.

9 L. Britnell, R. V. Gorbachev, R. Jalil, B. D. Belle, F. Schedin, A. Mishchenko, T. Georgiou, M. I. Katsnelson, L. Eaves, S. V. Morozov, N. M. R. Peres, J. Leist, A. K. Geim, K. S. Novoselov and L. A. Ponomarenko, *Science*, 2012, **335**, 947–950.

10 K. Roy, M. Padmanabhan, S. Goswami, T. P. Sai, G. Ramalingam, S. Raghavan and A. Ghosh, *Nat. Nanotechnol.*, 2013, **8**, 826–830.

11 Y. Sata, R. Moriya, S. Morikawa, N. Yabuki, S. Masubuchi and T. Machida, *Appl. Phys. Lett.*, 2015, **107**, 023109.

12 M. D. Tran, S.-G. Lee, S. Jeon, S.-T. Kim, H. Kim, V. L. Nguyen, S. Adhikari, S. Woo, H. C. Park, Y. Kim, J.-H. Kim and Y. H. Lee, *ACS Nano*, 2020, **14**, 13905–13912.

13 D. Luo, J. Tang, X. Shen, F. Ji, J. Yang, S. Weathersby, M. E. Kozina, Z. Chen, J. Xiao, Y. Ye, T. Cao, G. Zhang, X. Wang and A. M. Lindenberg, *Nano Lett.*, 2021, **21**, 8051–8057.

14 J. He, N. Kumar, M. Z. Bellus, H. Y. Chiu, D. He, Y. Wang and H. Zhao, *Nat. Commun.*, 2014, **5**, 5622.

15 L. Yuan, T. F. Chung, A. Kuc, Y. Wan, Y. Xu, Y. P. Chen, T. Heine and L. B. Huang, *Sci. Adv.*, 2018, **4**, e1700324.

16 S. Aeschlimann, A. Rossi, M. Chavez-Cervantes, R. Krause, B. Arnoldi, B. Stadtmuller, M. Aeschlimann, S. Forti, F. Fabbri, C. Coletti and I. Gierz, *Sci. Adv.*, 2020, **6**, eaay0761.

17 C. Ferrante, G. D. Battista, L. E. P. Lopez, G. Batignani, E. Lorchat, A. Virga, S. Berciaud and T. Scopigno, *Proc. Natl. Acad. Sci. U. S. A.*, 2022, **119**, e2119726119.

18 Y. Tan, X. B. Liu, Z. L. He, Y. R. Liu, M. W. Zhao, H. Zhang and F. Chen, *ACS Photonics*, 2017, **4**, 1531–1538.

19 H. Z. Zhou, Y. Z. Chen and H. M. Zhu, *Sci. Adv.*, 2021, **7**, eabg2999.

20 P. Valencia-Acuna, F. Rudayni, K. Rijal, W. L. Chan and H. Zhao, *ACS Nano*, 2023, **17**, 3939–3947.

21 R. J. Scott, P. Valencia-Acuna and H. Zhao, *ACS Nano*, 2023, **17**, 25368–25376.

22 A. Y. Lu, H. Y. Zhu, J. Xiao, C. P. Chuu, Y. M. Han, M. H. Chiu, C. C. Cheng, C. W. Yang, K. H. Wei, Y. M. Yang, Y. Wang, D. Sokaras, D. Nordlund, P. D. Yang, D. A. Muller, M. Y. Chou, X. Zhang and L. J. Li, *Nat. Nanotechnol.*, 2017, **12**, 744–749.

23 J. Zhang, S. Jia, I. Kholmanov, L. Dong, D. Q. Er, W. B. Chen, H. Guo, Z. H. Jin, V. B. Shenoy, L. Shi and J. Lou, *ACS Nano*, 2017, **11**, 8192–8198.

24 Y.-C. Lin, C. Liu, Y. Yu, E. Zarkadoula, M. Yoon, A. A. Puretzky, L. Liang, X. Kong, Y. Gu, A. Strasser, H. M. Meyer, M. Lorenz, M. F. Chisholm, I. N. Ivanov, C. M. Rouleau, G. Duscher, K. Xiao and D. B. Geohegan, *ACS Nano*, 2020, **14**, 3896.

25 M. M. Petric, M. Kremser, M. Barbone, Y. Qin, Y. Sayyad, Y. X. Shen, S. Tongay, J. J. Finley, A. R. Botello-Mendez and K. Muller, *Phys. Rev. B*, 2021, **103**, 035414.

26 D. B. Trivedi, G. Turgut, Y. Qin, M. Y. Sayyad, D. Hajra, M. Howell, L. Liu, S. J. Yang, N. H. Patoary, H. Li, M. M. Petric, M. Meyer, M. Kremser, M. Barbone, G. Soavi, A. V. Stier, K. Muller, S. Z. Yang, I. S. Esqueda, H. L. Zhuang, J. J. Finley and S. Tongay, *Adv. Mater.*, 2020, **32**, 2006320.

27 T. Zheng, Y.-C. Lin, Y. L. Yu, P. Valencia-Acuna, A. A. Puretzky, R. Torsi, C. Z. Liu, I. N. Ivanov, G. Duscher, D. B. Geohegan, Z. H. Ni, K. Xiao and H. Zhao, *Nano Lett.*, 2021, **21**, 931–937.

28 T. Zheng, Y.-C. Lin, N. Rafizadeh, D. B. Geohegan, Z. Ni, K. Xiao and H. Zhao, *ACS Nano*, 2022, **16**, 4197–4205.

29 J.-B. Wu, M.-L. Lin, X. Cong, H.-N. Liu and P.-H. Tan, *Chem. Soc. Rev.*, 2018, **47**, 1822–1873.

30 Z. H. Ni, H. M. Wang, J. Kasim, H. M. Fan, T. Yu, Y. H. Wu, Y. P. Feng and Z. X. Shen, *Nano Lett.*, 2007, 7, 2758–2763.

31 S. B. Harris, Y.-C. Lin, A. A. Puretzky, L. Liang, O. Dyck, T. Berlijn, G. Eres, C. M. Rouleau, K. Xiao and D. B. Geohegan, *ACS Nano*, 2023, **17**, 2472–2486.